The Astrophysical Journal, 825:43 (14pp), 2016 July 1 doi:10.3847/0004-637X/825/1/43

NON-AXISYMMETRIC PERPENDICULAR DIFFUSION OF CHARGED PARTICLES AND THEIR TRANSPORT ACROSS TANGENTIAL MAGNETIC DISCONTINUITIES

R. D. Strauss[1,2], J. A. le Roux[2,3], N. E. Engelbrecht[1], D. Ruffolo[4], and P. Dunzlaff[1]
[1] Center for Space Research, North-West University, Potchefstroom, 2522, South Africa; dutoit.strauss@nwu.ac.za
[2] Center for Space Plasma and Aeronomic Research, University of Alabama in Huntsville, Huntsville, AL 3585, USA
[3] Department of Space Science, University of Alabama in Huntsville, Huntsville, AL 35899, USA
[4] Department of Physics, Faculty of Science, Mahidol University, Bangkok 10400, Thailand
Received 2016 February 16; revised 2016 April 28; accepted 2016 April 29; published 2016 June 27

ABSTRACT

We investigate the transport of charged particles across magnetic discontinuities, focusing specifically on stream interfaces associated with co-rotating interaction regions in the solar wind. We argue that the magnetic field fluctuations perpendicular to the magnetic discontinuity, and usually also perpendicular to the mean magnetic field, are strongly damped in the vicinity of such a magnetic structure, leading to anisotropic perpendicular diffusion. Assuming that perpendicular diffusion arises from drifts in a turbulent magnetic field, we adopt a simplified approach to derive the relevant perpendicular diffusion coefficient. This approach, which we believe gives the correct principal dependences as expected from more elaborate calculations, allows us to investigate transport in different turbulent geometries, such as longitudinal compressional turbulence that may be present near the heliopause. Although highly dependent on the (possibly anisotropic) perpendicular length scales and turbulence levels, we generally find perpendicular diffusion to be strongly damped at magnetic discontinuities, which may in turn provide an explanation for the large particle gradients associated with these structures.

Key words: cosmic rays – diffusion – solar wind – Sun: heliosphere – Sun: magnetic fields – turbulence

1. INTRODUCTION

Co-rotating interaction regions (CIRs) form when alternating fast and slow solar wind regions interact and the resulting structure co-rotates with the Sun (e.g., Balogh et al. 1999; Gosling & Pizzo 1999). A schematic representation of a CIR is shown in Figure 1, also illustrating the structure of the CIR itself: a fast solar wind stream flows into a slow solar wind region forming a forward shock ahead of the CIR, while a reverse shock forms behind the CIR where faster plasma outruns the slower streams. In between the two shocks we usually find a stream interface (SI), which separates two different plasma populations: it is believed that the two regions adjacent to the SI are not magnetically connected and may even originate from different magnetic polarities in the solar corona. In any case, the SI can be regarded as a tangential discontinuity (e.g., Intriligator et al. 2001). See also Burlaga & Ness (1969) for a detailed discussion regarding tangential discontinuities.

In Figure 2 we show *Ulysses* observations of a CIR observed at ∼5 AU and mid-latitudes in late 1992 when the spacecraft was on its first southern descent toward the pole of the Sun after its Jupiter flyby in 1992 February. This is "CIR 8" in the CIR catalog of Wimmer-Schweingruber et al. (1997). The different panels, from top to bottom, show the magnetic field magnitude, the solar wind speed, and the particle fluxes as measured by the Low Energy Telescope (LET), the Kiel Electron Telescope (KET), and the High Energy Telescope (HET) detectors of the COsmic rays and Solar Particle INvestigation (COSPIN) experiment (Simpson et al. 1992). The LET measures the proton flux in the energy range of 0.9–1.2 MeV, while both the KET E4 channel and the HET H6 channel measure electrons in the energy ranges of 2.5–7 MeV and 1–3 MeV, respectively. The dominant contribution of MeV electrons is made by Jovian electrons (see, among others, Chenette 1980), while the low energetic proton flux can be attributed to shock-accelerated protons. The reverse shock is generally more effective in accelerating particles (Simnett & Roelof 1995), explaining the high proton flux in the region between the reverse shock and the SI. Before the passage of the CIR, *Ulysses* was located between the Jovian electron source and the CIR. A clear correlation between particles and the SI is evident: we observe a sudden drop in MeV electrons when the spacecraft crosses the SI and a simultaneous increase in shock-accelerated protons. This observation shows that *Ulysses* moved across a thin border that separates two different plasma regimes constituting an effective diffusion barrier.

Although it is well known that the shocks associated with CIRs accelerate particles and that CIRs are diffusion barriers for other cosmic ray (CR) species (e.g., Chenette 1980; Heber et al. 1997; McKibben et al. 1999; Kocharov et al. 2008), we believe that the role of the SI in influencing particle propagation is underappreciated (note in Figure 2 the large particle gradients directly at the SI) and needs to be reinvestigated. Moreover, CIRs give us the opportunity to investigate the role of tangential discontinuities in particle propagation in-situ; results that can be extended to other lesser known (explored) magnetic discontinuities and discontinuous magnetic structures, for instance, the heliopause (HP) or small-scale coherent structures in the solar wind (e.g., Tessein et al. 2013a, 2013b).

In this paper, we derive, using a simplified but illuminating approach, the functional form of the pitch-angle-dependent perpendicular diffusion coefficient for the most general turbulence scenario, after which we show how this coefficient and its pitch-angle dependence will change near a tangential discontinuity. For the sake of completeness, we also a give a more rigorous derivation for the pitch-angle-averaged perpendicular diffusion coefficient for expected turbulence conditions in the vicinity of a magnetic discontinuity.

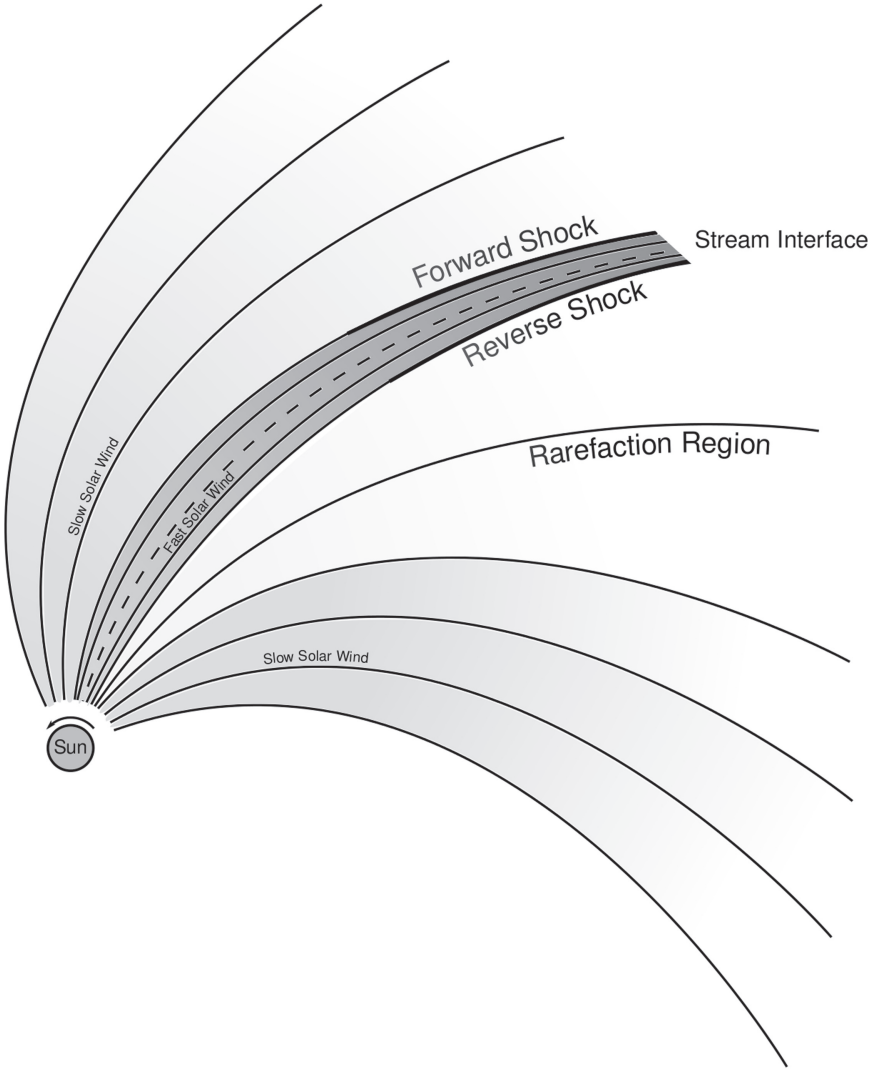

Figure 1. Schematic repesentation of a typical CIR.

2. THE SI AS A TANGENTIAL DISCONTINUITY AND IMPLICATIONS FOR PARTICLE TRANSPORT

In Figure 3 we zoom into the region close to the SI, identified in Figure 2, to show the magnetic topology near an SI. The dashed lines indicate the extent of the SI, which, in terms of magnetic field magnitude, can be identified by two almost discontinuous changes in the B_N component (for the observations we use the *RTN* coordinate system with *R* pointing in the radial direction, *T* in the longitudinal direction, and *N* completing the right-handed coordinate system pointing in the polar direction). When examining the azimuth λ and declination δ of the magnetic field, the SI for this scenario is a rotational discontinuity. This is a special case of a more general tangential discontinuity as discussed by Burlaga & Ness (1969), where the magnetic field vector rotates from a negative to a positive polarity (for a Parker 1958 magnetic field near Jupiter, $\pm\lambda \approx 75°$–$80°$ and $\delta \approx 0°$). Significantly, the observations seem consistent with an SI plane that includes the *N* direction.

Previous work focused on calculating turbulence quantities in CIRs (e.g., Crooker et al. 1999; Horbuty & Schmidt 1999), but the focus was on the entire CIR, whereas we are interested in possible turbulence changes close to the SI. For the 1 s resolution data, binned and shown in Figure 3, we calculate the variance in 1 minute intervals for each magnetic field component following the approach of, e.g., Forsyth et al. (1996), and show the resulting ratios $\delta B^2/B^2$, referred to as the turbulence ratios, in Figure 4 as the gray lines on an arbitrary scale (the lines are offset to one another to make the temporal behavior more clear). The calculation is done for the total magnetic field and separately for the different magnetic field components, $\delta B_i^2/B^2$, $i \in \{R, T, N\}$. The thick lines show 10 minute running averages of these quantities, while the dashed lines again identify the extent of the SI. Without knowing the three-dimensional (3D) structure of the SI, we assume that the normal of the SI surface lies in the *RT* plane, and look for a reduction in the fluctuation levels of the *N*-component. If the geometry of the average magnetic field is a Parker spiral, it would follow that any fluctuations in the observed B_θ-component, and hence in the *N*-component, would be almost purely turbulent in nature (see, e.g., Zank et al. 1996; Smith et al. 2001). In Figure 3, a clear reduction in B_N can be seen in the SI, while in Figure 4 we see a reduction in the variance in all three components in the SI. This behavior then constitutes a clear indication of a decrease in turbulence in the SI, even though from such a simple analysis no hard conclusions can be drawn as to the geometry of the transverse turbulent fluctuations, i.e., whether or not they are

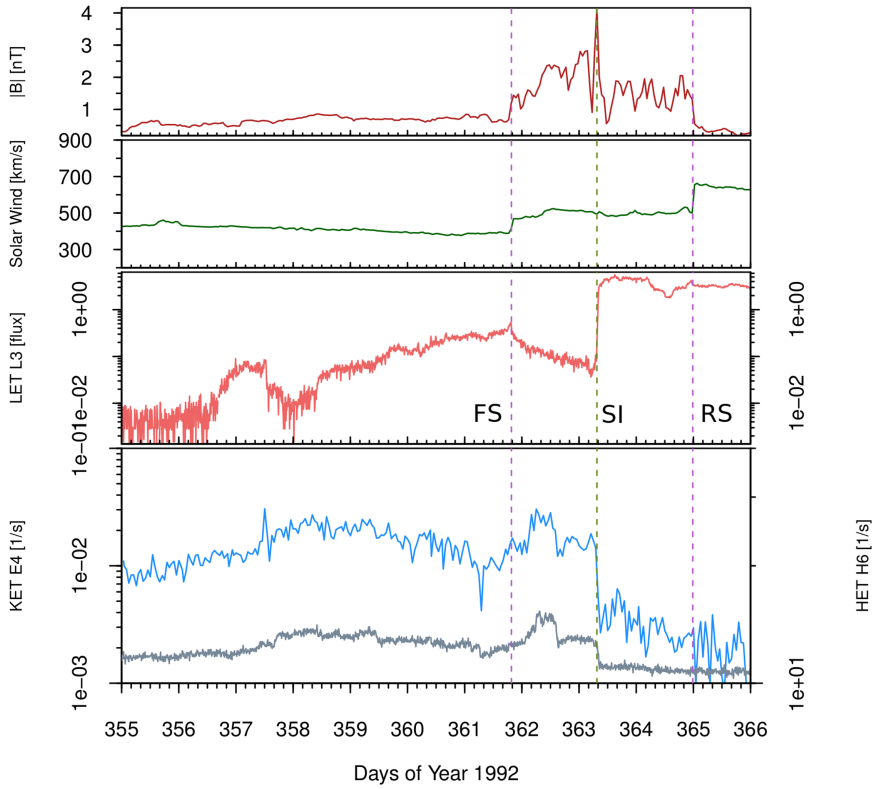

Figure 2. *Ulysses* observations of a typical CIR. The vertical dashed lines show, from left to right, the passage of the forward shock (FS), the stream interface (SI), and the reverse shock (RS) past the spacecraft. See the text for more details.

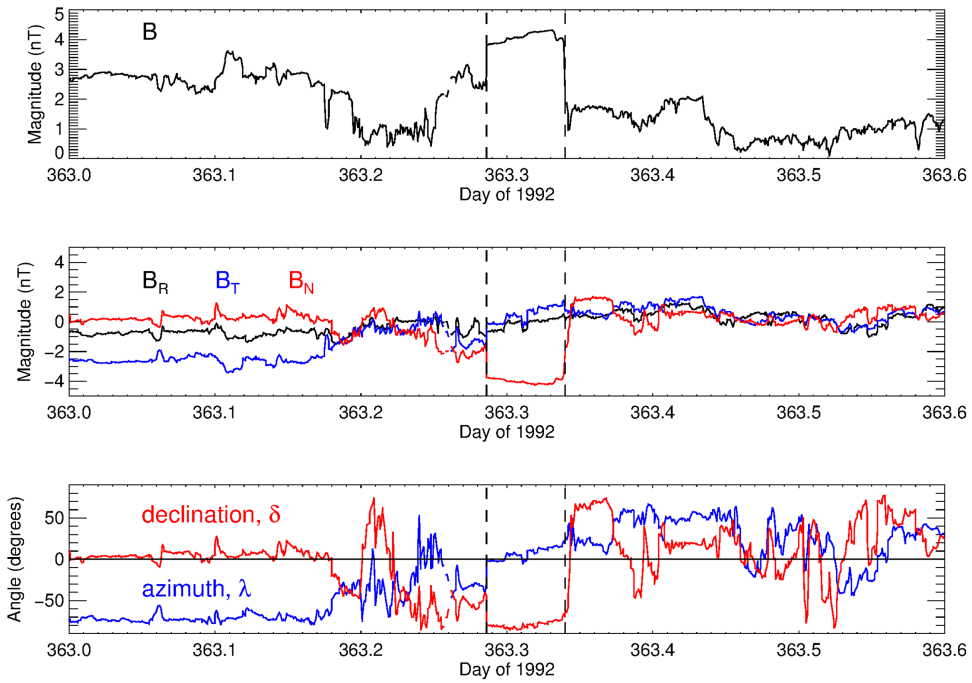

Figure 3. Close-up view of the region close to the SI identified in Figure 2. The dashed lines show the assumed extent of the SI.

axisymmetric. However, a geometrical argument for this can be proposed: because there is no plasma flow across a tangential discontinuity, the magnetic field component perpendicular to this interface should tend to zero, while also damping fluctuations perpendicular to such a surface. Schematically, this idea is illustrated in Figure 5, where we show a projection of diffusing (random walking) field lines under normal solar wind conditions in the left panel, while the right panel shows the expected scenario close to a tangential discontinuity (indicated by the red line): the field fluctuations perpendicular to the discontinuity should be damped, resulting in a more laminar structure (see also the discussion by, e.g., Intriligator et al. 2001, among others).

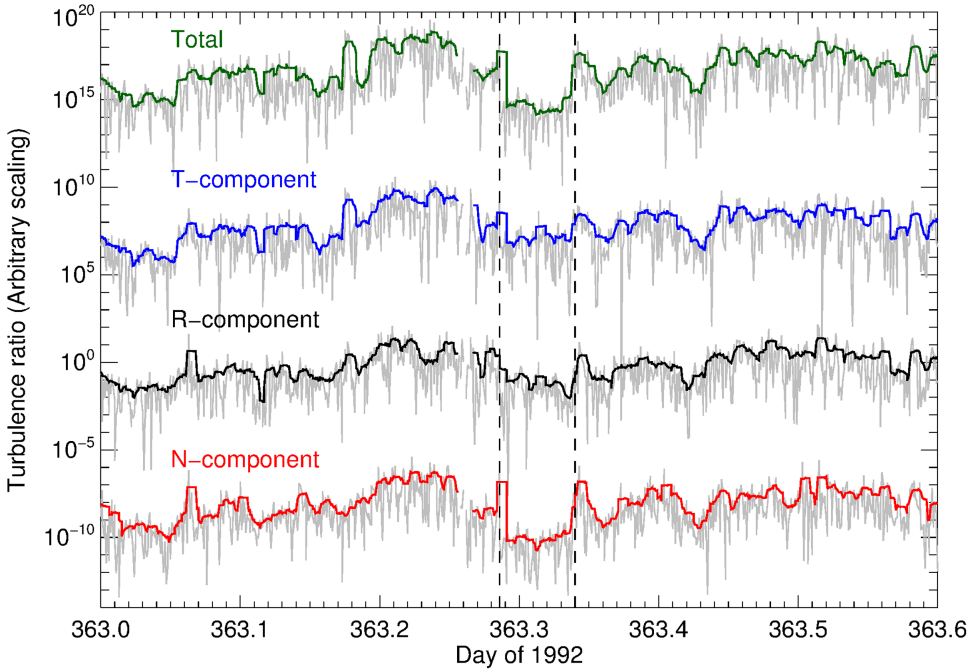

Figure 4. Ratio $\delta B^2/B^2$ (referred to as the turbulence ratio) calculated for the total magnetic field and the dfferent components ($\delta B_i^2/B^2$, $i \in \{R, T, N\}$) separately. Note that an arbitrary scale is used. The dashed lines again indicate the assumed extent of the SI. Thin gray lines show $\delta B^2/B^2$, calculated in 1 minute intervals, while the thick lines show 10 minute running averages.

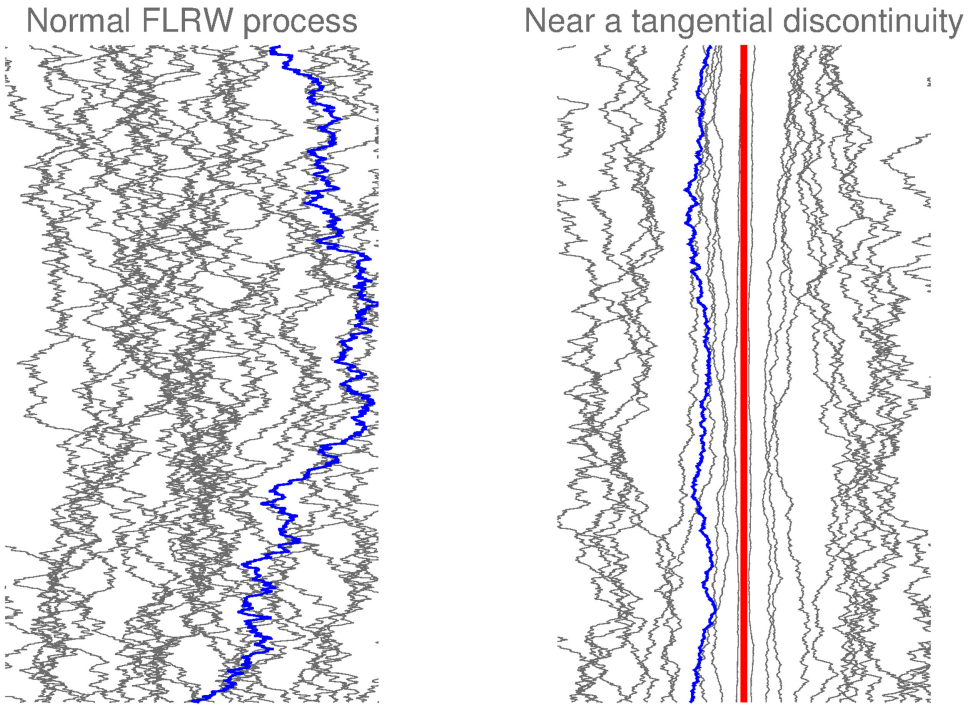

Figure 5. Schematic representation of the damping of magnetic field fluctuations close to a tangential discontinuity: under normal slar wind conditions (left panel), field lines undergo the normal randm walk process, while close to a discontinuity (indicated by the red line in the right panel), field lines cannot cross the discontinuous surface, and hence, the fluctuating component perpendicular to the discontinuity must also be damped. The blue lines indicate possible trajectories of particles along these wandering field lines. The figure is taken from Strauss et al. (2015).

The fluctuations parallel to the discontinuity should, however, remain unaffected. The blue lines in Figure 5 show the possible trajectories of particles along these wandering field lines, indicating that damped fluctuations would, to first order, also damp (inhibit) diffusion across the discontinuity.

3. PERPENDICULAR DIFFUSION IN TURBULENT MAGNETIZED PLASMAS

In most existing scattering theories, only the pitch-angle-averaged perpendicular diffusion coefficient, $\kappa_\perp$, is calculated (Matthaeus et al. 2003; Shalchi 2009), which is related to the

pitch-angle dependent perpendicular diffusion coefficient $D_\perp$ by

$$\kappa_\perp = \frac{1}{2}\int_{-1}^{1} D_\perp(\mu)d\mu, \tag{1}$$

where μ is the cosine of the pitch-angle (Schlickeiser 2002). For some CR modeling applications, however, knowing $D_\perp$ is essential; for example, Strauss & Fichtner (2015) have shown that for solar energetic particle propagation, where an anisotropic distribution is modeled, the functional dependence of $D_\perp$ on pitch-angle is extremely important and that choosing ad hoc forms for this dependence can lead to very different results, i.e., very different levels of perpendicular diffusion, even if the resulting $\kappa_\perp$'s are the same. This effect is illustrated in more detail in Section 7. Similarly, $D_\perp$ cannot as yet be derived very easily from first principles for more exotic (meaning, different from near-Earth solar wind conditions) turbulence regimes. An example of such conditions would be the compressive nature of fluctuations observed in the outer heliosphere (e.g., Burlaga et al. 2014) or close to magnetic discontinuities. With this in mind, we present a simplified, order-of-magnitude derivation of $D_\perp$ for different turbulent geometries, which, we believe, gives the correct principle dependence of $D_\perp$ on μ. These expressions can serve as a basis for modelers to simulate CR transport in these regimes and will most likely in future be replaced by more detailed derivations.

Charged particles are scattered by the turbulent irregularities present in the solar wind, leading to diffusion both parallel and perpendicular to the mean field. To include the effect of turbulence, it is useful to decompose the resulting magnetic field, $\boldsymbol{B}$, into an average, locally uniform background field, $B_0\hat{z}$, and a static, random turbulent component

$$\boldsymbol{B} = B_0\hat{z} + \boldsymbol{b}(x, y, z), \tag{2}$$

with an ensemble average

$$\langle \boldsymbol{b} \rangle = 0, \tag{3}$$

and $\langle b^2 \rangle \equiv \delta B^2$ with $\langle \delta B^2 \rangle$ the variance. The static turbulence assumption is made because we assume that energetic particles (CRs) will see decorrelated magnetic fields on a timescale $\tau_{\rm dec} \ll \tau_c$ where τ_c is the turbulence dynamical timescale. For a fully 3D fluctuating component, $\boldsymbol{b}$, is given by

$$\boldsymbol{b} = b_x(x, y, z)\hat{x} + b_y(x, y, z)\hat{y} + b_z(x, y, z)\hat{z}, \tag{4}$$

which contains both transverse (to the mean field, $B_0\hat{z}$) components ($b_{x,y}$) and a parallel component (b_z), and may, in principle, depend on any of the spatial coordinates (x, y, z). By assuming only transverse fluctuations and reduced turbulent geometries, Equation (4) can be simplified to e.g., a two-dimensional (2D) or slab geometry (see, e.g., Shalchi 2009 for a review). We will, however, keep the 3D geometry of $\boldsymbol{b}$ and calculate an approximate expression for the perpendicular diffusion coefficient, $D_\perp(\mu)$, on the pitch-angle level. As usual, the fluctuating components are assumed to be weak

$$b_{x,y,z} \ll B_0. \tag{5}$$

We use the TGK (Taylor–Green–Kubo) formulation to calculate the perpendicular mean square displacement (e.g., Taylor 1922; Green 1951; Kubo 1957)

$$\langle \Delta x_\perp^2 \rangle = \int_0^{\Delta t} dt' \int_0^{\Delta t} dt'' \langle v_\perp(t')v_\perp(t'') \rangle, \tag{6}$$

where $\langle v_\perp(t')v_\perp(t'') \rangle$ is the perpendicular component of the two-time velocity correlation function. By assuming homogeneous, magnetosonic fluctuations, we have, at late times, an estimate of $D_\perp$

$$D_\perp(\mu) = \lim_{\Delta t\to\infty} \frac{\langle \Delta x_\perp^2 \rangle}{2\Delta t} = \int_0^\infty dt' \langle v_\perp(0)v_\perp(t') \rangle. \tag{7}$$

By furthermore assuming that the velocity correlation function decays exponentially with time (inspired by e.g., Bieber & Matthaeus 1991),

$$\langle v_\perp(0)v_\perp(t) \rangle = \langle v_\perp^2(0) \rangle e^{-\frac{t}{\tau_{\rm dec}}}, \tag{8}$$

and where $\tau_{\rm dec}$ represents the characteristic timescale of decay, $D_\perp$ can quite simply be described by

$$D_\perp(\mu) = \langle v_\perp^2 \rangle \tau_{\rm dec}. \tag{9}$$

In deriving Equation (9), it was assumed that $\tau_{\rm dec}$ does not have any time dependence. The following paragraph will, however, show $\tau_{\rm dec}$ to be pitch-angle-dependent, and μ does change time-dependently due to continuous pitch-angle scattering along the trajectory of a particle. This is a process we therefore neglect in this derivation. If pitch-angle diffusion was to be included in the above derivation, it would yield, at late times, the isotropic diffusion coefficient $\kappa_\perp$, whereas we are interested in calculating the instantaneous Fokker–Planck coefficient $D_\perp$. Note that a similar assumption is made by, e.g., Qin & Shalchi (2014), where they assumed dominant perpendicular diffusion (with respect to pitch-angle scattering). Alternatively, it can be argued that our derivation is only valid on shorter timescales where μ can be approximated to be constant.

If $v_\perp$ is now interpreted as the component of the guiding center drift velocity across the mean field (see Fraschetti & Jokipii 2011; Fraschetti 2015), we may set $v_\perp = ({}_gV)_\perp$, so that

$${}_gV \approx \overbrace{v_\parallel \boldsymbol{e}_B}^{\text{streaming}} + \overbrace{\boldsymbol{V}_E}^{E\text{-field}} + \overbrace{\frac{p_\perp v_\perp}{2qB}\frac{\boldsymbol{B}\times\nabla B}{B^2}}^{\text{gradient}} + \overbrace{\frac{p_\parallel v_\parallel}{qB}\boldsymbol{e}_B \times \nabla_\parallel \boldsymbol{e}_B}^{\text{curvature}}, \tag{10}$$

keeping terms up to first order in small quantities assuming $r_L \ll l$, where l is the turbulence correlation scale, and $v_\parallel \gg V_E$. In Equation (10), $\mathbf{e}_B$ is a unit vector pointing along $\boldsymbol{B}$, $\perp$, and $\parallel$ referring to the parallel and perpendicular components of the particle velocity and momentum ($\boldsymbol{p}$), q is the particle charge, and $\boldsymbol{V}_E$ is the electric field drift velocity. The resulting guiding center drift velocity component, projected in

the direction perpendicular to B_0, is approximately

$$ {}_gV_x \approx v\left\{\begin{array}{l} \overbrace{\mu\frac{b_x}{B_0}}^{\text{streaming}} + \overbrace{\sqrt{\Gamma}\frac{V_A}{v}\frac{b_x}{B_0}}^{E\text{-field}} \\ \overbrace{-\frac{1}{2}\frac{r_L}{l_y}(1-\mu^2)\left(\frac{b_\perp^2}{B_0^2}+\frac{b_z}{B_0}\right)}^{\text{gradient}} - \overbrace{\frac{r_L\mu^2}{l_z}\frac{b_y}{B_0}}^{\text{curvature}} \end{array}\right\}\hat{x} \quad (11) $$

and

$$ {}_gV_y \approx v\left\{\begin{array}{l} \overbrace{\mu\frac{b_y}{B_0}}^{\text{streaming}} + \overbrace{\sqrt{\Gamma}\frac{V_A}{v}\frac{b_y}{B_0}}^{E\text{-field}} \\ \overbrace{+\frac{1}{2}\frac{r_L}{l_x}(1-\mu^2)\left(\frac{b_\perp^2}{B_0^2}+\frac{b_z}{B_0}\right)}^{\text{gradient}} + \overbrace{\frac{r_L\mu^2}{l_z}\frac{b_x}{B_0}}^{\text{curvature}} \end{array}\right\}\hat{y}, \quad (12) $$

in the x and y directions, respectively. Here, we have introduced the scale lengths $l_{x,y,z}$ such that, e.g.,

$$ \frac{\partial b_y}{\partial x} \approx \frac{b_y}{l_x}, \quad (13) $$

and shortened notation by using

$$ b_\perp^2 = b_x^2 + b_y^2. \quad (14) $$

Furthermore, $r_{\rm L}$ is the maximal Larmor radius, $V_{\rm A}$ the Alfvén speed, and Γ is the ratio of kinetic to magnetic energies in the fluctuations ($\Gamma = 1$ for Alfvénic fluctuations).

First, let us assume that particles see decorrelated turbulence by propagating *across* $\boldsymbol{B}_0$. Given the assumption of weak turbulence, we assume that particles can complete a perpendicular turbulence correlation length $\langle l_{x,y}\rangle$ without significant gyro-orbit distortion by scattering from gyro-resonant wave–particle interactions with microscale turbulence ($\tau_{\rm sc} \gg \tau_{\rm cross}$, where $\tau_{\rm sc}$ is the scattering time due to gyro-resonant interaction with microscale turbulence, and $\tau_{\rm cross}$ is the time particles need to cross a length $\langle l_{x,y}\rangle$). Thus, we assume that particles see decorrelated turbulence by moving a perpendicular correlation scale across $\boldsymbol{B}_0$, e.g., for the y-component

$$ \tau_{\rm dec} = \frac{\langle l_y\rangle}{\langle {}_gV_y^2\rangle^{1/2}}, \quad (15) $$

so that the components of the potentially anisotropic diffusion coefficient, $D_\perp$, becomes

$$ D_x(\mu) = \langle l_x\rangle\langle {}_gV_x^2\rangle^{1/2},\ D_y(\mu) = \langle l_y\rangle\langle {}_gV_y^2\rangle^{1/2}. \quad (16) $$

In Section 6 we also consider that particles with nearly undisturbed gyro-orbits see decorrelated turbulence by propagating a parallel turbulence correlation scale $\langle l_x\rangle$ along $\boldsymbol{B}_0$.

4. SCENARIO 1: TRANSVERSE FLUCTUATIONS

First, we show in Section 4.1 that our simplified approach, when applied to axisymmetric fluctuations, can reproduce the field line random walk (FLRW; Jokipii 1966) limit of $D_\perp$ for which the μ dependence is well known. Further below in Section 4.2, we generalize the result to non-axisymmetric fluctuations. Following previous authors, we assume transverse fluctuations ($b_z = 0$) and a 2D geometry for these fluctuations (see, e.g., Shalchi 2009, and references therein). In our notation, the latter requires that terms related to curvature drift be neglected in Equations (11) and (12); that is,

$$ \frac{b_{x,y}}{l_z} = 0, \quad (17) $$

because $l_z \to \infty$. We also neglect electric field drift (for fast particles with $v \gg V_A$).

4.1. Axisymmetric Fluctuations

By assuming axisymmetric fluctuations, we require that $l_\perp = l_x = l_y$ and $b = b_x = b_y$, for which $D_\perp$ reduces to

$$ \begin{aligned} D_\perp &\approx v\langle l_\perp\rangle\left\langle\left(\mu\frac{b}{B_0} \mp \frac{r_L}{l_\perp}(1-\mu^2)\frac{b^2}{B_0^2}\right)^2\right\rangle^{1/2} \\ &\approx v\langle l_\perp\rangle|\mu|\frac{\langle b^2\rangle^{1/2}}{B_0} + vr_L(1-\mu^2)\frac{\langle b^2\rangle}{B_0^2}, \end{aligned} \quad (18) $$

if $\langle b^3\rangle = \langle b^2\rangle\langle b\rangle = 0$. Furthermore, by assuming that $r_L \ll l_\perp$, we end up recovering the classical FLRW limit for 2D turbulence when particles follow randomly walking field lines with undisturbed gyro-orbits given by

$$ D_\perp(r_L \ll l_\perp) \approx v\langle l_\perp\rangle|\mu|\frac{\langle b^2\rangle^{1/2}}{B_0}. \quad (19) $$

A further comparison with, e.g., Qin & Shalchi (2014) shows that we do indeed recover the correct principle dependences of $D_\perp$. In the framework of Qin & Shalchi (2014), based on the unified nonlinear transport theory of Shalchi (2010), an expression similar to Equation (19) results when pitch-angle diffusion is neglected. The fact that Equation (19) does correspond, at least in a qualitative fashion, with the more rigorously derived expressions for $D_\perp$ available in the literature gives us some confidence in our simplified approach.

4.2. Non-axisymmetric Fluctuations

We now apply the general expression derived in the previous section to the SI of CIR (as an example of a tangential discontinuity). The discontinuity is assumed to be in the x–z plane, so that y is both perpendicular to the mean field and the discontinuity itself. Referring to the idealized picture presented in Figure 5, we assume the most extreme case of $b_y = 0$, directly at the discontinuous surface, and proceed to calculate $D_\perp$ as

$$ D_x \approx v\langle l_x\rangle\left\langle\left(\mu\frac{b_x}{B_0} + \frac{1}{2}\frac{r_L}{l_y}(1-\mu^2)\frac{b_x^2}{B_0^2}\right)^2\right\rangle^{1/2} \quad (20) $$

and

$$ D_y \approx v\frac{r_L}{2}\frac{\langle l_y\rangle}{\langle l_x\rangle}(1-\mu^2)\frac{\langle b_x^2\rangle}{B_0^2}, \quad (21) $$

which now, not unexpectedly, leads to anisotropic perpendicular diffusion; the y-component is expected to be damped,

while the x component (being perpendicular to the mean field but parallel to the surface) should remain unchanged.

We can again assume $r_L \ll l_x$ (low-energy particles that tend to follow large-scale fluctuating field lines), leading to

$$D_x(r_L \ll l_x) \approx v|\mu|\langle l_x\rangle \frac{\langle b_x^2\rangle^{1/2}}{B_0} \tag{22}$$

and

$$D_y(r_L \ll l_x) \approx 0. \tag{23}$$

Equations (22) and (23) are in perfect agreement with Figure 5: the FLRW process is completely damped in the y direction for this idealized set-up, while being totally unaffected in the x direction.

We end up with $D_y \ll D_x$, so that the presence of the discontinuity leads, in the limits considered, to a very effective diffusion barrier: essentially D_y is heavily suppressed, thereby suppressing perpendicular diffusion across the discontinuity and leading to the large particle gradients across this discontinuous surface as shown in Figure 1.

We may generalize the above expression by introducing the (assumed) fixed ratios

$$b_y = \alpha b_x \Rightarrow b_\perp^2 = (1+\alpha^2)b_x^2 \tag{24}$$

and

$$l_y = \beta l_x \tag{25}$$

with, most likely, $\alpha < 1$ and $\beta > 1$ near a discontinuity, leading to

$$\begin{aligned} D_x(\mu) &\approx v\langle l_x\rangle \left\langle \left(\mu\frac{b_x}{B_0} - \frac{1}{2}\frac{r_L}{l_x}(1-\mu^2)\frac{(1+\alpha^2)}{\beta}\frac{b_x^2}{B_0^2}\right)^2\right\rangle^{1/2}, \\ &\approx v|\mu|\langle l_x\rangle\frac{\langle b_x^2\rangle^{1/2}}{B_0} + \frac{(1+\alpha^2)}{\beta}v\frac{r_L}{2}(1-\mu^2)\frac{\langle b_x^2\rangle}{B_0^2} \end{aligned} \tag{26}$$

and

$$\begin{aligned} D_y(\mu) &\approx v\beta\langle l_x\rangle \left\langle \left(\mu\alpha\frac{b_x}{B_0} + \frac{1}{2}\frac{r_L}{l_x}(1-\mu^2)(1+\alpha^2)\frac{b_x^2}{B_0^2}\right)^2\right\rangle^{1/2}, \\ &\approx v\alpha\beta|\mu|\langle l_x\rangle\frac{\langle b_x^2\rangle^{1/2}}{B_0} + \beta(1+\alpha^2)v\frac{r_L}{2}(1-\mu^2)\frac{\langle b_x^2\rangle}{B_0^2} \end{aligned} \tag{27}$$

if, once again, $\langle b^3\rangle = 0$. These expressions form the basis for modeling the transport of particles, on the pitch-angle level, across magnetic discontinuities. This requires knowledge of both ratios α and β, which can, in principle, be derived from observations. Equations (26) and (27) are again qualitatively similar to the results of Fraschetti & Jokipii (2011), who found $\kappa_\perp$ to be comprised of two contributions: the FLRW coefficient and an additional contribution from guiding center motion.

An interesting possibility is also presented from the observational side: if pitch-angle scattering is weak enough, the pitch-angle dependence of D_y would imprint on the particle anisotropies beyond the discontinuity. If α is small enough in Equation (27), D_y peaks at $\mu = 0$ and these particles will have the highest mobility across the discontinuity and hence and excess of particles with $\mu = 0$ should be observable there (see also Strauss & Fichtner 2014 for a similar argument). Dwyer et al. (1997) presented observations of anisotropic particle distributions within the CIR, illustrating the importance of perpendicular diffusion on the pitch-angle level. For cases when pitch-angle scattering is efficient enough to isotropize the distribution, the isotropic formulation described in Section 8 can be used.

5. SCENARIO 2: LONGITUDINAL FLUCTUATIONS

In contrast to the transversal fluctuations normally assumed and observed close to Earth, the *Voyager 1* (*V1*) spacecraft observed the turbulence in the outer heliosphere (beyond the termination shock inside of the heliospheath) to be mainly compressible (longitudinal; Burlaga et al. 2014, 2015). The case of predominantly compressible turbulence can be handled quite easily in our framework by assuming $b_{x,y} \ll b_z$. The result is

$$D_x(\mu) \approx v\frac{r_L}{2}\frac{\langle l_x\rangle}{\langle l_y\rangle}(1-\mu^2)\frac{\langle b_z^2\rangle^{1/2}}{B_0} \tag{28}$$

and

$$D_y(\mu) \approx v\frac{r_L}{2}\frac{\langle l_y\rangle}{\langle l_x\rangle}(1-\mu^2)\frac{\langle b_z^2\rangle^{1/2}}{B_0}, \tag{29}$$

which reduce to $D_\perp = D_x = D_y$ if axisymmetric fluctuations ($l_x = l_y$) are again assumed. Interestingly, *V1* observed anisotropic energetic particle distributions beyond the HP in the local interstellar medium (Krimigis et al. 2013). Although the presence of anisotropic particle distributions in the local interstellar medium is not surprising (isotropization via pitch-angle scattering is expected to be very slow), the process for producing these anisotropies remains disputed. It was proposed by Strauss & Fichtner (2014) that a $D_\perp$ that obtains its maximum value at $\mu = 0$ could provide a natural explanation for such anisotropies; a postulate that is partially vindicated in this work through Equations (28) and (29).

The HP is also a tangential discontinuity (e.g., Florinski et al. 2013), separating solar and interstellar plasmas, and therefore, in a sense, similar to the SI of a CIR, except for the fact that the fluctuations appear to be mainly compressible. *V1* observations of CRs indicate that the HP is a diffusion barrier (e.g., Stone et al. 2013), again similar to SIs, and consistent with global CR models that require a damped $\kappa_\perp$ (e.g., Guo & Florinski 2014; Luo et al. 2015) to explain these observations. This would seem to indicate that, at least close to the HP, perpendicular diffusion in compressible turbulence across the HP is a very slow process and thus possibly anisotropic because the component perpendicular to the HP is again heavily suppressed based on our geometrical argument (see Figure 5 and its discussion above). We can see this in our theory for perpendicular diffusion in compressible turbulence by assuming suppressed turbulence perpendicular to the HP according to the condition $\langle l_y\rangle/\langle l_x\rangle \ll 1$ in Equations (28) and (29). Then it follows that $D_y(\mu) \ll D_x(\mu)$ so that perpendicular diffusion across the HP is suppressed compared to perpendicular diffusion along the HP.

6. SCENARIO 3: PERPENDICULAR DIFFUSION WITH PARALLEL DECORRELATION

So far we assumed that energetic particles will see decorrelated magnetic fields by propagating a turbulence correlation length across $\boldsymbol{B}_0$. However, when turbulence is weak, as assumed here, it is to be expected that particles will experience decorrelated fields first by propagating a turbulence correlation length *along* $\boldsymbol{B}_0$ if l_z is finite (i.e., a slab or longitudinal component must be present; see Section 4). This assumption is similar to the idea of "ballistic decorrelation" as proposed by Ruffolo et al. (2012). Therefore, we have

$$\tau_{\rm dec} = \frac{\langle l_z \rangle}{\langle {}_g V_z^2 \rangle^{1/2}}, \tag{30}$$

where ${}_g V_z \approx v|\mu| + v_p$, and $v_p \geqslant 0$ is the wave phase speed associated with low-frequency MHD turbulence. For example, for Alvénic turbulence, $v_p{=}V_{\rm A}$, so that particles will see decorrelated turbulence due to turbulence dynamics on a timescale $\tau_c = \langle l_z \rangle / V_A$, ignoring the effect of particle propagation. So far we assumed static turbulence, but will now include decorrelation due to turbulence dynamics to avoid a blowup in $D_\perp(\mu)$ at $\mu = 0$. Accordingly,

$$D_x(\mu) = \frac{\langle l_z \rangle \langle {}_g V_x^2 \rangle}{v|\mu| + v_p}, \; D_y(\mu) = \frac{\langle l_z \rangle \langle {}_g V_y^2 \rangle}{v|\mu| + v_p}, \tag{31}$$

where ${}_g V_{x,y}$ is given by Equations (11) and (12). Upon assuming that the turbulence component at and perpendicular to the interface of the discontinuity (e.g., the SI of a CIR) $b_y \to 0$, which also implies that $l_y \to \infty$, we find that

$$D_x(\mu) \approx v \langle l_z \rangle |\mu| \frac{\langle b_x^2 \rangle}{B_0^2}, \tag{32}$$

for $v\mu \gg v_p$, and

$$D_y(\mu) \approx \frac{v \langle l_z \rangle}{|\mu| + v_p/v} \left\langle \left(\frac{1}{2} \frac{r_L}{l_x} (1 - \mu^2) \times \left(\frac{b_x^2}{B_0^2} + \frac{b_z}{B_0} \right) + \frac{r_L}{l_z} \mu^2 \frac{b_x}{B_0} \right)^2 \right\rangle. \tag{33}$$

Thus, we see that for perpendicular diffusion along the SI, $D_x(\mu)$, we recover the familiar FLRW limit for which $D_x(\mu) \propto |\mu|$. The μ dependence for perpendicular diffusion across the SI, $D_y(\mu)$, is determined by a competition between gradient and curvature drift, and also depends on gyro-motion along $\boldsymbol{B}_0$.

If the turbulence geometry is dominated by a 2D transverse component, $b_z \ll b_x$ and $l_z \gg l_x$, we find that

$$D_y(\mu) \approx \frac{1}{4} v r_L^2 \frac{\langle l_z \rangle}{\langle l_x \rangle^2} \frac{(1 - \mu^2)^2}{|\mu| + v_p/v} \frac{\langle b_x^2 \rangle^2}{B_0^4}. \tag{34}$$

Whereas before, in the case of perpendicular decorrelation, we found $D_y(\mu) \propto (1 - \mu^2)$, for parallel decorrelation $D_y(\mu) \propto (1 - \mu^2)^2/(|\mu| + v_p/v)$, indicating that perpendicular diffusive transport at $\mu = 0$ is strongly accentuated across the SI. Comparing $D_x(\mu)$ and $D_y(\mu)$ again confirms that $D_y(\mu) \ll D_x(\mu)$, taking into account weak turbulence and $r_L \ll l_x$ as guiding center theory requires.

Keeping in mind that turbulence tends to be compressible (longitudinal) at the HP interface, we again assume the limit of pure longitudinal turbulence, $b_{x,y} \to 0$ and $l_{x,y} \to \infty$. Since we already applied $b_y = 0$, $l_y \to \infty$ to derive Equations (32) and (33), only $b_x \to 0$ and $l_x \to \infty$ is needed. Then $D_x(\mu) \approx 0$ and $D_y(\mu) \approx 0$. However, *V1* observations (Burlaga et al. 2014) suggest that the transverse component is significant so that $l_x \to \infty$ is too severe. Instead, we assume predominantly compressible turbulence, where $b_z \gg b_x$ and $l_z < l_x$. Then,

$$D_y(\mu) \approx \frac{1}{4} v r_L^2 \frac{\langle l_z \rangle}{\langle l_x \rangle^2} \frac{(1 - \mu^2)^2}{|\mu| + v_p/v} \frac{\langle b_z^2 \rangle}{B_0^2} \ll D_x(\mu) \tag{35}$$

and we recover the same strong dependence $D_y(\mu) \propto (1 - \mu^2)^2/(|\mu| + v_p/v)$ as in the limit of predominantly transverse turbulence, but an expression that is more suitable for energetic particle transport across the HP interface.

7. AN ILLUSTRATIVE EXAMPLE

To illustrate how important the choice of the functional form of $D_\perp$ can be for particle transport models, consider the following ad hoc forms:

$$\begin{aligned} D_\perp^{(\#1)} &= D_{\perp,0} \\ D_\perp^{(\#2)} &= 2D_{\perp,0}|\mu| \\ D_\perp^{(\#3)} &= \frac{3}{2} D_{\perp,0}(1 - \mu^2) \\ D_\perp^{(\#4)} &= \chi D_{\perp,0} \frac{(1 - \mu^2)^2}{|\mu| + \Pi}, \end{aligned} \tag{36}$$

with $D_{\perp,0}$ and χ constants, the latter given by

$$\frac{1}{\chi} = \frac{1}{12}[24(\Pi - 1)^2(\Pi + 1)^2 \coth^{-1}(1 + 2\Pi) - 12\Pi^3 + 6\Pi^2 + 20\Pi - 9], \tag{37}$$

and $\Pi = v_p/v$. The different choices for $D_\perp$ in Equation (36) can be interpreted as being due to (from top to bottom): #1 the pitch-angle dependence assumed to have no importance, #2 the FLRW process, #3 scattering in compressional fluctuations, and #4 when considering parallel decorrelation. These coefficients are plotted as a function of pitch-angle in Figure 6 to illustrate how very different their functional forms are. Note that we assume $\Pi = 0.01$. It is interesting to note that for each of these four cases the calculated isotropic diffusion coefficient is $\kappa_\perp = D_{\perp,0}$. One may therefore naively think that these four cases should therefore also affect particle transport in the same fashion.

To illustrate that this is definitely not the case, we incorporate these coefficients into the pitch-angle-dependent toy model of Strauss & Fichtner (2014), where an isotropic particle distribution propagates across a tangential discontinuity into a region of weak pitch-angle scattering (this is similar to anomalous CRs diffusing across the HP into the interstellar medium). Results from this model are shown in Figure 7 in terms of sector diagrams, i.e., the intensity versus pitch-angle. It is clear that for this choice of model set-up the particle distributions beyond the discontinuity are still anisotropic, but, more importantly, they are not identical: the FLRW coefficient result (#2) is almost isotropic, while the parallel decorrelation coefficient (#4) result shows, as expected, the largest level of

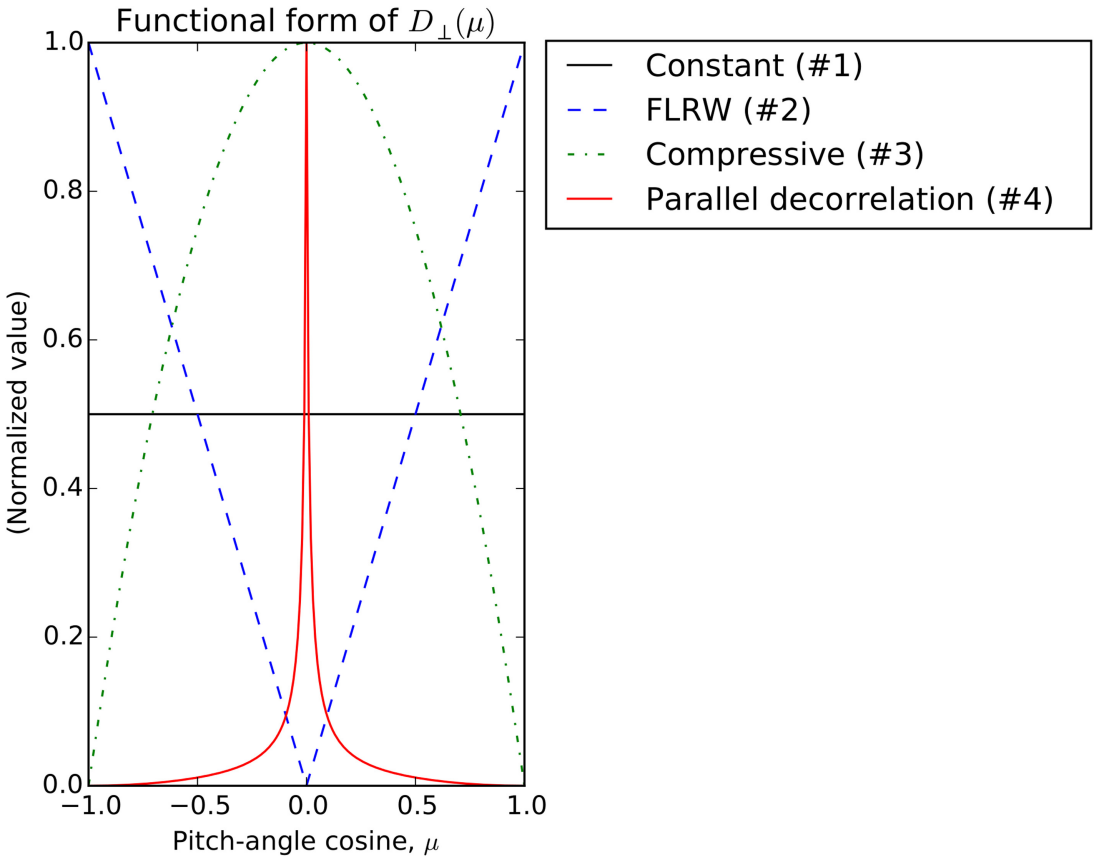

Figure 6. Four ad hoc choices of $D_\perp$ used to illustrate the importance of the functional form (pitch-angle dependence) of this coefficients. Note that although these coefficients have vastly different pitch-angle dependencies, they all lead to the same value of the isotropic perpendicular diffusion coefficient $\kappa_\perp$.

anisotropy. For each panel in this figure, we have also calculated the value of the omni-directional intensity (the isotropic intensity averaged over pitch-angle) and added this as the thick purple lines. Interestingly, even the value of the omni-directional intensity varies significantly between model set-up.

This section therefore illustrates that the pitch-angle dependence of $D_\perp$ is an important modeling parameter, and that choosing its functional form in an ad hoc fashion can lead to very different modeling results.

8. PITCH-ANGLE-AVERAGED PERPENDICULAR DIFFUSION IN NON-AXISYMMETRIC TURBULENCE

When looking at timescales longer than $\sim\lambda_{||}/v$, where $\lambda_{||}$ is the isotropic parallel mean-free path, the particle distribution will be isotropized, and the transport of such distributions can be described by the pitch-angle-averaged value of the perpendicular diffusion coefficient. To obtain $\kappa_\perp$, we can, in principle, make use of the results of the proceeding sections for $D_\perp$ and simply average these over pitch-angle (see Equation (1)). However, recent years have seen a surge in the development of theories to describe the asymptotic diffusion of charged particles in turbulent plasmas (see, e.g., Matthaeus et al. 2003; Shalchi 2009, 2010; Ruffolo et al. 2012, and Qin & Zhang 2014) and all of these are more elaborate and well tested than our rather simplified approach outlined earlier. Hence, instead of simply applying Equation (1), we choose to calculate $\kappa_\perp$ using a well-established nonlinear diffusion theory, as discussed below. Although some of the above-mentioned theories have been applied to the study of galactic CR modulation (see, e.g., Engelbrecht & Burger 2013), to the best of our knowledge the application of these theories to scenarios such as that described in the introduction to this work has not yet occurred. Therefore, the implied non-axisymmetry of magnetic fluctuations near a tangential magnetic discontinuity provides an ideal scenario in which to apply a more ab initio approach to modeling the transport of energetic particles. In this section, we employ the nonlinear guiding center (NLGC) theory of Matthaeus et al. (2003) with the random ballistic decorrelation interpretation presented by Ruffolo et al. (2012) to derive pitch-angle-averaged expressions for perpendicular diffusion coefficients in non-axisymmetric 2D turbulence. The use of this scattering theory presents one significant advantage over other NLGC-type theories in the literature, as not only does it agree well with numerical simulations of the perpendicular diffusion coefficients in axisymmetric turbulence, but it also directly yields expressions for perpendicular mean-free paths that are not implicit functions of themselves. This latter point is of considerable advantage should such expressions be employed in numerical models. When generalized to non-axisymmetric turbulence, the results of this section again show that perpendicular diffusion across a SI is suppressed.

Assuming composite turbulence (see, e.g., Bieber et al. 1994) for the case where transverse fluctuations are both anisotropic and axisymmetric, the perpendicular diffusion coefficients (taking into account a correction for potential particle backtracking) can be calculated using (Ruffolo

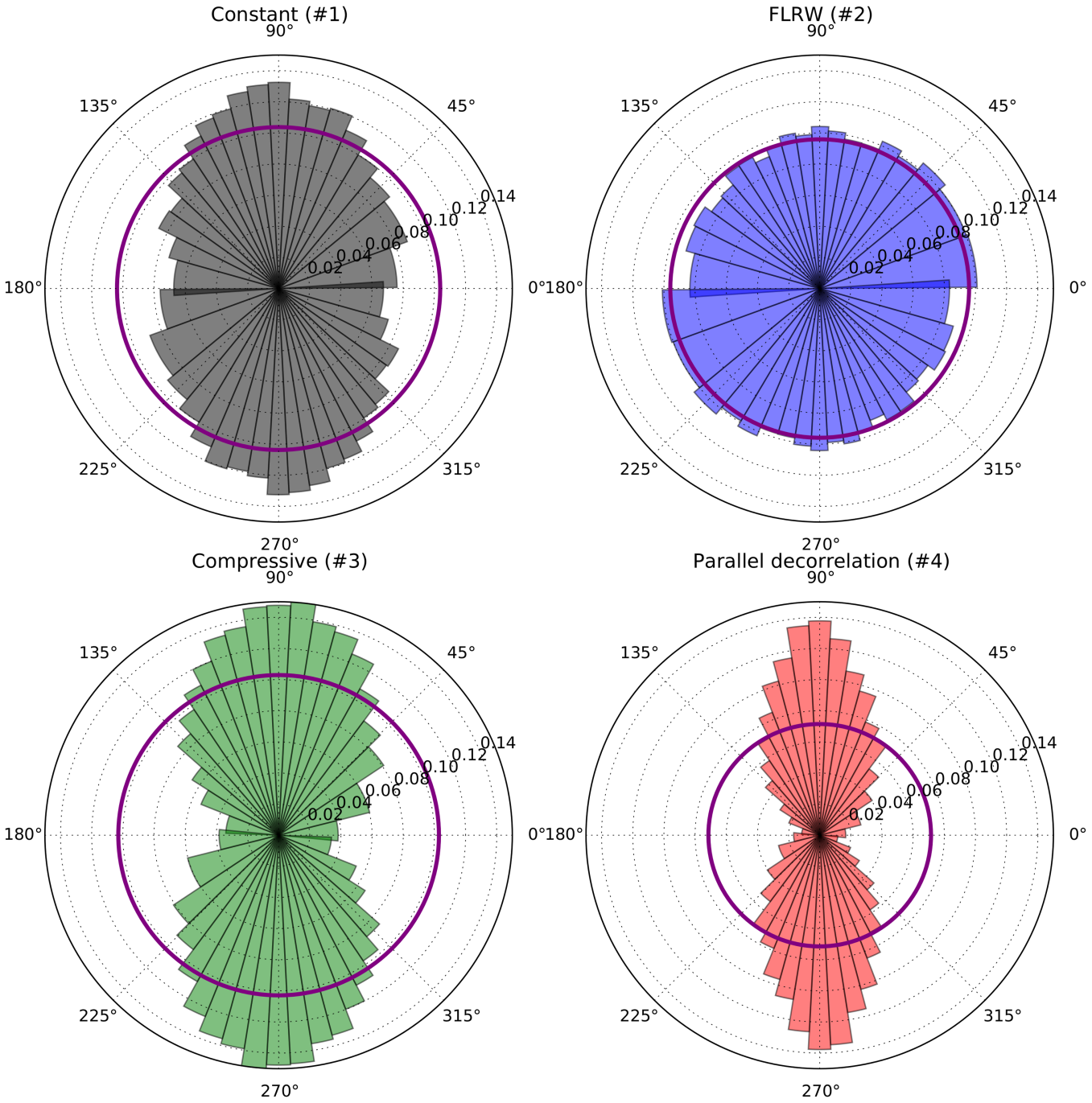

Figure 7. Resulting particle distributions, plotted as sector diagrams (i.e., intensity vs. pitch-angle) when the coefficients (shown in Figure 6) are incorporated into the toy model of Strauss & Fichtner (2014). The thick purple lines show, for each scenario, the value of the omni-directional (isotropic) intensity which also differ for the different scenarios.

et al. 2012)

$$\kappa_{xx} = \frac{a^2 v^2}{3B_0^2}\sqrt{\frac{\pi}{2}}\int \frac{S_{xx}^{2D}(\boldsymbol{k})}{\sqrt{\Sigma_i k_i^2 \langle \tilde{v}_i^2 \rangle}}\,\mathrm{erfc}(\alpha)d\boldsymbol{k},$$
$$\kappa_{yy} = \frac{a^2 v^2}{3B_0^2}\sqrt{\frac{\pi}{2}}\int \frac{S_{yy}^{2D}(\boldsymbol{k})}{\sqrt{\Sigma_i k_i^2 \langle \tilde{v}_i^2 \rangle}}\,\mathrm{erfc}(\alpha)d\boldsymbol{k}, \quad (38)$$

where B_o is the uniform background magnetic field magnitude, v the particle velocity, and $S_{ii}^{2D}(k_x, k_y)$ the 2D modal power spectrum associated with the field component $i = x$ or y. Furthermore, the quantity a^2 is a constant, various interpretations of which can be found in, e.g., Shalchi & Dosch (2008) and Shalchi (2015). In the present study, it is assumed that $a^2 = 1/3$, after Matthaeus et al. (2003). The quantity α is given by

$$\alpha = \frac{v^2/3\kappa_{zz} + \gamma(\boldsymbol{k})}{\sqrt{2\Sigma_i k_i^2 \langle \tilde{v}_i^2 \rangle}}, \quad (39)$$

with κ_{zz} being the diffusion coefficient along B_o, and $\gamma(\boldsymbol{k})$ is a damping function set to zero in this study, as magnetostatic

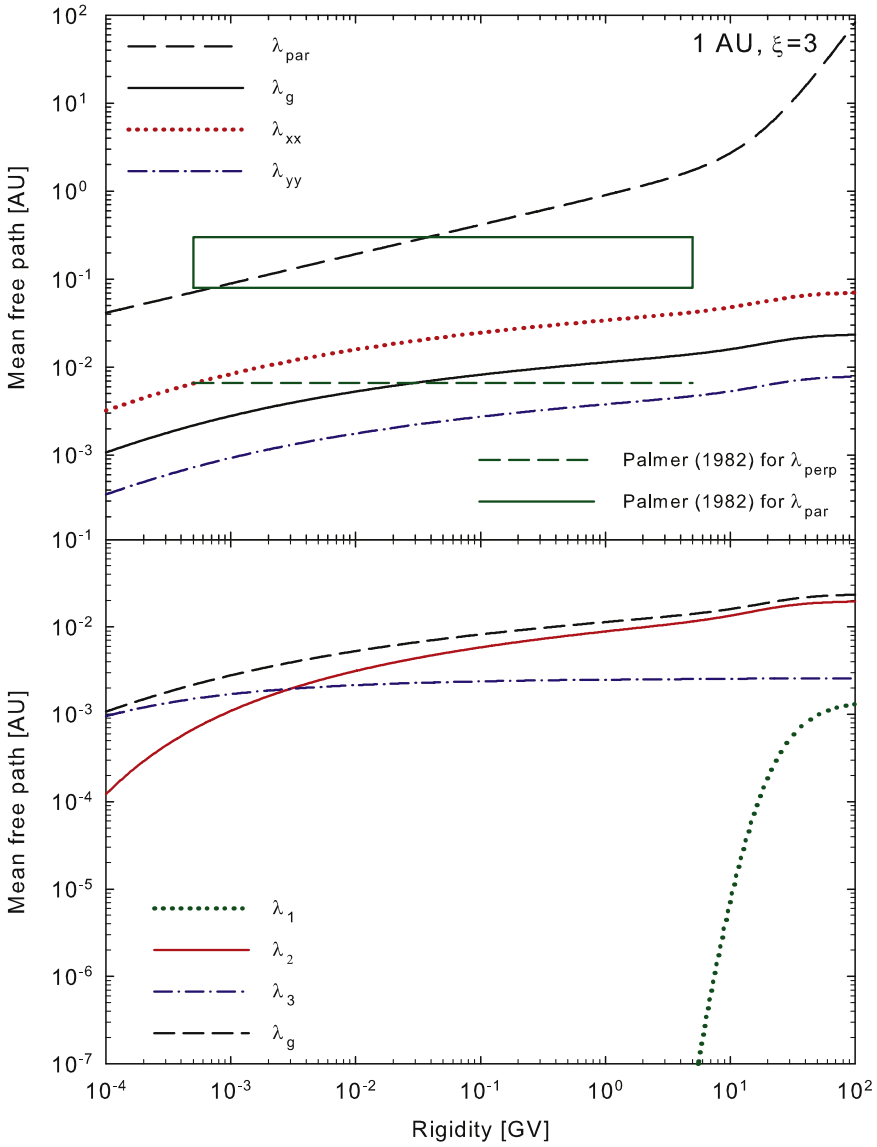

Figure 8. Top panel: mean perpendicular mean-free path λ_g (see Equation (44)) as well as perpendicular mean-free paths λ_{xx} and λ_{yy} as function of rigidity for non-axisymmetric 2D magnetic fluctuations with ellipticity factor $\xi = 3$. The parallel mean-free path used as input for λ_g, as well as Palmer (1982) consensus ranges (green block for $\lambda_\parallel$, green dashed line for $\lambda_\perp$), are shown to guide the eye. Bottom panel: The various terms λ_i in Equation (44) as well as λ_g, as function of rigidity.

fluctuations are assumed. The components of the average square of the guiding center velocity $\langle \tilde{v}^2 \rangle$ can, in the presence of non-axisymmetric transverse magnetic fluctuations, be written in a way similar to that of Ruffolo et al. (2012) as

$$\langle \tilde{v}_x^2 \rangle = \frac{a^2 v^2}{3} \frac{\delta B_{T,x}^2}{B_o^2},$$

$$\langle \tilde{v}_y^2 \rangle = \frac{a^2 v^2}{3} \frac{\delta B_{T,y}^2}{B_o^2},$$

$$\langle \tilde{v}_z^2 \rangle = \frac{v^2}{3} - \langle \tilde{v}_x^2 \rangle - \langle \tilde{v}_y^2 \rangle = \frac{v^2}{3}\left(1 - \frac{\delta B_T^2}{B_o^2}\right), \quad (40)$$

where the velocity distribution is assumed to be isotropic, and $\delta B_T^2 = \delta B_{2D}^2 + \delta B_{sl}^2$ is assumed to be the total variance associated with transverse fluctuations. Note that the *direct* contribution of slab fluctuations to perpendicular diffusion is neglected in Equation (38), as implied by the numerical simulations of Qin et al. (2002a, 2002b; see Shalchi 2006 for more details). However, all transverse fluctuations are taken into account in Equation (40), such that, for example, $\delta B_{T,x}^2 = \delta B_{2D,x}^2 + \delta B_{sl,x}^2$, with the subscripts "2D" and "sl" denoting variances of 2D and slab fluctuations, respectively. This implicit dependence on the slab component exists alongside that implied by the parallel mean-free path dependence of Equation (39), where $\kappa_{zz} = v\lambda_\parallel/3$.

The power spectra of the non-axisymmetric fluctuations are treated following the approach of Ruffolo et al. (2006, 2008), as opposed to the more generalized approach of Weinhorst et al. (2008), for the purposes of simplicity. From the fact that 2D magnetic fluctuations can be written in terms of the curl of some potential function $a(x, y)$ such that $\boldsymbol{b}_{2D} = \nabla \times a(x, y)\boldsymbol{e}_z$, the 2D power spectra can be written as $S_{xx}^{2D} = k_y^2 A(k_x, k_y)$ and $S_{yy}^{2D} = k_x^2 A(k_x, k_y)$ (see, e.g., Matthaeus et al. 2007), where $A(k_x, k_y)$ is the power spectrum of $a(x, y)$. Ruffolo et al. (2006) define an ellipticity parameter ξ such that $A(k_x, k_y)$ is

constant along ellipses in k-space that have a k_y to k_x ratio of ξ. This would then be equivalent to the axisymmetric case, where $A(k_x, k_y)$ is constant along circles defined by $k_\perp = k_x^2 + k_y^2$ (Ruffolo et al. 2008), under the coordinate transformation $k_x' = \xi^{1/2} k_x$ and $k_y' = \xi^{-1/2} k_y$. Assuming that $\delta B_x^2 / \delta B_y^2$ is the same for slab and 2D components (see, e.g., Ruffolo et al. 2006), as might be expected for a generic suppression of turbulence in one direction, implies that $\delta B_{T,x}^2 / \delta B_{T,y}^2 = \xi^2$, which further implies that $\langle \tilde{v}_x^2 \rangle / \langle \tilde{v}_y^2 \rangle = \xi^2$. It remains now to write Equation (38) in such a way as to allow one to calculate expressions for κ_{ii} using some specified form for $S^{2D}(k_\perp') = k_\perp'^2 A(k_\perp')$. Following the approach of Ruffolo et al. (2008), one can define a geometric mean of the x and y components of the guiding center velocity such that $\langle \tilde{v}_g^2 \rangle = \sqrt{\langle \tilde{v}_x^2 \rangle \langle \tilde{v}_y^2 \rangle}$, with $\langle \tilde{v}_x^2 \rangle = \xi \langle \tilde{v}_g^2 \rangle$ and $\langle \tilde{v}_y^2 \rangle = \langle \tilde{v}_g^2 \rangle / \xi$, and the term $\sqrt{\Sigma_i k_i^2 \langle \tilde{v}_i^2 \rangle}$ becomes $k_\perp' \sqrt{\langle \tilde{v}_g^2 \rangle}$. Furthermore, taking into account that $S_{xx}^{2D} = k_y^2 A = \xi k_y'^2 A$ and $S_{yy}^{2D} = k_x^2 A = k_x'^2 A / \xi$ leads to

$$\kappa_g = \frac{a^2 v^2}{3 B_0^2} \sqrt{\frac{\pi}{2}} \int \frac{k_\perp'^2 A}{2 k_\perp' \sqrt{\langle \tilde{v}_g^2 \rangle}} \mathrm{erfc}\left(\frac{v^2 / 3 \kappa_{zz}}{k_\perp' \sqrt{2 \langle \tilde{v}_g^2 \rangle}} \right) d\boldsymbol{k}_\perp' = \frac{a^2 v^2}{3 B_0^2} \sqrt{\frac{\pi}{2}} \int \frac{S^{2D}(k_\perp')}{2 k_\perp' \sqrt{\langle \tilde{v}_g^2 \rangle}} \mathrm{erfc}\left(\frac{v^2 / 3 \kappa_{zz}}{k_\perp' \sqrt{2 \langle \tilde{v}_g^2 \rangle}} \right) d\boldsymbol{k}_\perp', \quad (41)$$

where $\kappa_g = \sqrt{\kappa_{xx} \kappa_{yy}}$. It then follows that $\kappa_{xx} = \xi \kappa_g$ and that $\kappa_{yy} = \kappa_g / \xi$.

Forms for $S^{2D}(K_\perp')$ can now be specified, allowing one to derive expressions for κ_{ii}. One such form is that employed by Engelbrecht & Burger (2013), which has an omni-directional power spectrum $\mathcal{E}(K_\perp') = 2\pi K_\perp' S^{2D}(K_\perp')$ in the inertial range with spectral range $\nu > 1$, a wavenumber-independent, energy-containing range, and a range at the lowest wavenumbers where $\mathcal{E}$ goes as $k_\perp'^q$ for $q > 0$. This last range is included based on physical arguments by Matthaeus et al. (2007). This spectrum is given by

$$S^{2D}(K_\perp') = g_0 \begin{cases} (\lambda_{\mathrm{out}} k_\perp')^q, & |k_\perp'| < \lambda_{\mathrm{out}}^{-1}; \\ 1, & \lambda_{\mathrm{out}}^{-1} \leqslant |k_\perp'| < \lambda_{2D}^{-1}; \\ (\lambda_{2D} k_\perp')^{-\nu}, & |k_\perp'| \geqslant \lambda_{2D}^{-1}. \end{cases} \quad (42)$$

where $g_0 = (C_0 \lambda_{2D} \delta B_{2D}^2) / (2\pi k_\perp')$, and

$$C_0 = \left[1 - \frac{q}{1+q} \left(\frac{\lambda_{2D}}{\lambda_{\mathrm{out}}} \right) + \frac{1}{\nu - 1} \right]^{-1} \quad (43)$$

with λ_{2D} and λ_{out} denoting length scales associated with the wavenumbers at which the inertial and energy-containing ranges commence, respectively. Equation (41) can then be evaluated using the MATHEMATICA program with Equation (42) as input. Due to the piecewise definition of Equation (42), this yields an expression of the form

$$\lambda_g = \lambda_1 + \lambda_2 + \lambda_3, \quad (44)$$

where $\lambda = 3\kappa / v$, and

$$\begin{aligned} \lambda_1 &= \frac{x_0}{q} \left(\sqrt{3\epsilon} B_o a \lambda_\parallel \mathrm{erfc}\,(x_1) - \frac{3 B_o^2 \lambda_{\mathrm{out}}}{\sqrt{2\pi}} E_{(q+1)/2}(x_1^2) \right), \\ \lambda_2 &= x_0 \left(\frac{3 B_o^2 \sqrt{2}}{\sqrt{\pi}} [\lambda_{2D} x_2 - \lambda_{\mathrm{out}} x_3] + \sqrt{3\epsilon} B_o a \lambda_\parallel \log \frac{\lambda_{\mathrm{out}}}{\lambda_{2D}} \right), \\ \lambda_3 &= \frac{x_0}{\nu} \sqrt{3\epsilon} B_o a \lambda_\parallel \left(\mathrm{erfc}\,(x_4) + \frac{1}{\sqrt{\pi} x_4^\nu} \left[\Gamma\left(\frac{\nu+1}{2} \right) - \Gamma\left(\frac{\nu+1}{2}, x_4^2 \right) \right] \right), \end{aligned} \quad (45)$$

with $\epsilon = \sqrt{\delta B_{T,x}^2 \delta B_{T,y}^2}$, and, for notational convenience,

$$\begin{aligned} x_0 &= \sqrt{\frac{\pi}{2}} \frac{C_0 \lambda_{2D} \delta B_{2D}^2}{2 B_o^2 \epsilon \lambda_\parallel}, \\ x_1 &= \sqrt{\frac{3}{2}} \frac{B_o \lambda_{\mathrm{out}}}{a \sqrt{\epsilon} \lambda_\parallel}, \\ x_2 &= {}_2F_2\left(\frac{1}{2}, \frac{1}{2}; \frac{3}{2}, \frac{3}{2}; -x_4^2 \right), \\ x_3 &= {}_2F_2\left(\frac{1}{2}, \frac{1}{2}; \frac{3}{2}, \frac{3}{2}; -x_1^2 \right), \\ x_4 &= \sqrt{\frac{3}{2}} \frac{B_o \lambda_{2D}}{a \sqrt{\epsilon} \lambda_\parallel}. \end{aligned}$$

Note that $E_{(q+1)/2}$ denotes the exponential integral function, ${}_2F_2$, a hypergeometric function, with erf and erfc the error function and the complimentary error function, respectively. Note also that Γ with one or two arguments denotes the gamma or incomplete gamma function, respectively.

The top panel of Figure 8 shows the mean-free paths discussed above evaluated as functions of rigidity (particle momentum per charge) with an ellipticity parameter $\xi = 3$ for 1 AU solar minimum turbulence parameters, with Palmer (1982) consensus ranges (green block for $\lambda_\parallel$, green dashed line for $\lambda_\perp$) to guide the eye. The values employed for the 2D and slab correlation scales are those reported by Weygand et al. (2011) for the solar wind near Earth, and it is assumed that $\lambda_{\mathrm{out}} = 100 \lambda_{2D}$. The total variance $\delta B_T^2 = \delta B_{sl}^2 + \delta B_{2D}^2$ is taken to be 12 nT^2, from Smith et al. (2006), and $B_o = 5$ nT. Lastly, it is assumed that $\nu = 5/3$, and that $q = 3$. An expression for the parallel mean-free path $\lambda_\parallel$ is needed to evaluate the above expressions. To this end, the quasilinear theory result for parallel scattering due to slab fluctuations derived by Teufel & Schlickeiser (2003) and employed by, e.g., Burger et al. (2008), is used as a first approach. This expression is given by

$$\lambda_\parallel = \frac{3s}{\sqrt{\pi}(s-1)} \frac{R^2}{k_m} \left(\frac{B_o}{\delta B_{sl}} \right)^2 \left[\frac{1}{4\sqrt{\pi}} + \frac{2R^{-s}}{\sqrt{\pi}(2-s)(4-s)} \right], \quad (46)$$

where $R = R_L k_m$, in terms of the maximal proton gyroradius R_{L} and the wavenumber k_m associated with the slab turnover scale λ_{sl}. This expression is derived assuming a slab fluctuation spectrum with a flat energy-containing range, and an inertial range with spectral index $s = 5/3$. Note that turbulence quantities pertaining to the slab fluctuations are denoted by the

subscript "sl." From the top panel of Figure 8, all perpendicular mean-free paths gradually increase with increasing rigidity, with λ_g in the ballpark of the Palmer consensus range for the parameters employed. With an ellipticity factor of $\xi = 3$, the perpendicular mean-free path associated with one direction perpendicular to the background magnetic field (red line, subscript "xx") is clearly larger than that associated with the other perpendicular direction (blue line, subscript "yy"). In particular, $\lambda_{xx}/\lambda_{yy} = \xi^2$, which is consistent with results from the direct numerical simulations of Ruffolo et al. (2008). The various terms in Equation (44) are shown as function of rigidity in the bottom panel of Figure 8. As is the case for perpendicular mean-free paths derived using NLGC-type theories (see, e.g., Shalchi et al. 2010 and Shalchi 2013), the contribution from the term resulting from the integration over the energy-containing range predominates beyond ~2 MV, which covers the range of rigidities of interest to CR modulation studies. The term corresponding to the inertial range contributes little to λ_g for these 1 AU parameters at high rigidities, but becomes more significant at lower rigidities, eventually predominating below ~2 MV. Lastly, the term corresponding to the integration over the lowest wavenumber range on the power spectrum very rapidly becomes very small as rigidity decreases, and its contribution is negligible even at 100 GV.

9. DISCUSSION

In this work, we presented a relatively straightforward simplified derivation of $D_\perp$ on the pitch-angle level. We have shown that, at least in some limits, this approach gives the correct principle dependences of $D_\perp$, especially its dependence on μ. Such an approach allows us to investigate particle transport in more exotic (as compared to near-Earth conditions) turbulence geometries, such as compressional turbulence that may be present in the outer heliosphere. We have also generalized our results for the case of anisotropic perpendicular diffusion, where the anisotropy can be due to either the level of the turbulent fluctuations, or the correlation scales being anisotropic. Such a scenario may present itself near SIs associated with CIRs, where the presence of the magnetic discontinuity can presumably damp fluctuations perpendicular to both the mean magnetic field and the magnetic structure itself. This last assumption leads to perpendicular diffusion across the magnetic discontinuity to be heavily suppressed, which may explain the large particle gradients observed at these structures.

It was also shown by modifying the scattering theory proposed by Ruffolo et al. (2012) that the asymptotic (pitch-angle-averaged) diffusion coefficient in the perpendicular direction along which transverse magnetic fluctuations are damped is reduced accordingly. This supports our conclusion that non-axisymmetry of the fluctuations retards the progress of particles across the SI. Novel expressions for such asymptotic diffusion coefficients were derived, which in the future could also prove useful in numerical studies of the transport of such particles, not only in the presence of CIRs, but also wherever transverse turbulence may prove to be non-axisymmetric in the heliosphere at large.

The key to reduced transport across magnetic discontinuities is therefore the damping of perpendicular fluctuations. Here, we have used a geometrical argument to show that it should indeed be the case, while we provided an initial analysis of a CIR to show some observational support for this argument. A more rigorous data analysis is needed to confirm this assumption, especially focusing on the nature of the turbulence near SIs.

This work is based on the research supported in part by the National Research Foundation (NRF) of South Africa (R.D.S. is supported through the Thuthuka Program; grant No. 87998). Opinions expressed and conclusions arrived at are those of the authors and are not necessarily to be attributed to the NRF. R.D.S. acknowledges partial financial support from the Fulbright Visiting Scholar Program. D.R. is supported through the Basic Research Grant BRG5880009 from the Thailand Research Fund. J.A.l.R. acknowledges support from NASA grants NNX14AF43G and NNX15AI65G.

REFERENCES

Balogh, A., Bothmer, V., Crooker, N. U., et al. 1999, SSRv, 89, 141
Bieber, J. W., & Matthaeus, W. H. 1991, Proc. 22nd ICRC (Dublin), 3, 248
Bieber, J. W., Matthaeus, W. H., & Smith, C. W. 1994, ApJ, 420, 294
Burger, R. A., Krüger, T. P. J., Hitge, M., & Engelbrecht, N. E. 2008, ApJ, 674, 511
Burlaga, J. F., & Ness, N. F. 1969, SoPh, 9, 467
Burlaga, L. F., Florinski, V., & Ness, N. F. 2015, ApJL, 804, L31
Burlaga, L. F., Ness, N. F., Florinski, V., & Heerikhuisen, J. 2014, ApJ, 792, 134
Chenette, D. L. 1980, JGR, 85, A5
Crooker, N. U., Gosling, J. T., Bothmer, V., et al. 1999, SSRv, 89, 179
Dwyer, J. R., Mason, G. M., Mazur, J. E., et al. 1997, ApJL, 490, L115
Engelbrecht, N. E., & Burger, R. A. 2013, ApJ, 772, 46
Florinski, V., Jokipii, J. R., Alouani-Bibi, F., & le Roux, J. A. 2013, ApJL, 776, L37
Forsyth, R. J., Horbury, T. S., Balogh, A., & Smith, E. C. 1996, GeoRL, 23, 595
Fraschetti, F. 2015, arXiv:1512.08973
Fraschetti, F., & Jokipii, J. R. 2011, ApJ, 734, 83
Gosling, J. T., & Pizzo, V. J. 1999, SSRv, 89, 21
Green, M. S. 1951, JChPh, 19, 1036
Guo, X., & Florinski, V. 2014, ApJ, 793, 18
Heber, B., et al. 1997, in Proc. 31st ESLAB Symp. on Correlated Phenomena at the Sun, in the Heliosphere and in Geospace, ed. A. Wilson (European Space Agency), 331
Horbuty, T. S., & Schmidt, J. M. 1999, SSRv, 89, 61
Intriligator, D. A., Jokipii, J. R., Horbury, T. S., et al. 2001, JGR, 106, A6
Jokipii, J. R. 1966, ApJ, 146, 480
Kocharov, L., Laivola, J., Mason, G. M., Didkovsky, L., & Judge, D. L. 2008, ApJ, 176, 497
Krimigis, S. M., Decker, R. B., & Roelof, E. C. 2013, Sci, 341, 144
Kubo, R. 1957, JPSJ, 12, 570
Luo, X., Zhang, M., Potgieter, M. S., Xueshang, F., & Pogorelov, N. V. 2015, ApJ, 808, 82
Matthaeus, W. H., Bieber, J. W., Ruffolo, D., Chuychai, P., & Minnie, J. 2007, ApJ, 667, 956
Matthaeus, W. H., Qin, G., Bieber, J. W., & Zank, G. P. 2003, ApJL, 590, L53
McKibben, R. B., Jokipii, J. R., Burger, R. A., et al. 1999, SSRv, 89, 307
Palmer, I. D. 1982, RvGSP, 20, 335
Parker, E. N. 1958, ApJ, 128, 664
Qin, G., Matthaeus, W. H., & Bieber, J. W. 2002a, ApJL, 578, L117
Qin, G., Matthaeus, W. H., & Bieber, J. W. 2002b, GeoRL, 29, 1048
Qin, G., & Shalchi, A. 2014, ApPhR, 6, 1
Qin, G., & Zhang, L.-H. 2014, ApJ, 787, 12
Ruffolo, D., Chuychai, P., & Matthaeus, W. H. P. 2006, ApJ, 644, 971
Ruffolo, D., Chuychai, P., Wongpan, P., et al. 2008, ApJ, 686, 1231
Ruffolo, D., Pianpanit, T., Matthaeus, W. H., & Chuychai, P. 2012, ApJL, 747, L34
Schlickeiser, R. 2002, Cosmic Ray Astrophysics (Berlin: Springer)
Shalchi, A. 2006, A&A, 453, L43
Shalchi, A. 2009, Nonlinear Cosmic Ray Diffusion Theories (Berlin: Springer)
Shalchi, A. 2010, ApJL, 720, L127
Shalchi, A. 2013, ApJ, 774, 7

Shalchi, A. 2015, AdSpR, 56, 1264
Shalchi, A., & Dosch, A. 2008, ApJ, 685, 971
Shalchi, A., Li, G., & Zank, G. P. 2010, Ap&SS, 325, 99
Simnett, G. M., & Roelof, E. C. 1995, SSRv, 72, 303
Simpson, J. A., Anglin, J. D., Balogh, A., et al. 1992, A&AS, 92, 363
Smith, C. W., Isenberg, P. A., Matthaeus, W. H., & Richardson, J. D. 2006, ApJ, 638, 508
Smith, W. S., Matthaeus, W. H., Zank, G. P., et al. 2001, JGR, 106, 8253
Stone, E. C., Cummings, A. C., McDonald, F. B., et al. 2013, Sci, 341, 150
Strauss, R. D., & Fichtner, H. 2014, A&A Lett., 572, L3
Strauss, R. D., & Fichtner, H. 2015, ApJ, 801, 29
Strauss, R. D., Fichtner, H., Potgieter, M. S., et al. 2015, JPhCS, 642, 012026
Taylor, G. I. 1922, Proc. Lond. Math. Soc., 20, 196
Tessein, J. A., et al. 2013a, ApJL, 776, L8
Tessein, J. A., et al. 2013b, ApJ, 812, 68
Teufel, A., & Schlickeiser, R. 2003, A&A, 397, 15
Weinhorst, B., Shalchi, A., & Fichtner, H. 2008, ApJ, 677, 671
Weygand, J. M., Matthaeus, W. H., Dasso, S., & Kivelson, M. G. 2011, JGR, 116, A08102
Wimmer-Schweingruber, R. F., von Steiger, R., & Paerli, R. 1997, JGR, 102, 17407
Zank, G. P., Matthaeus, W. H., & Smith, C. W. 1996, JGR, 101, 17093